NUMERICAL MODELING OF STORM SURGES, WIND WAVES AND FLOODING IN THE TAGANROG BAY

Vladimir Fomin, Marine Hydrophysical Institute of RAS, Russia
Dmitrii Alekseev, Marine Hydrophysical Institute of RAS, Russia
Dmitrii Lazorenko, Marine Hydrophysical Institute of RAS, Russia

fomin.dntmm@gmail.com

Storm surges and wind waves are ones of the most important hydrological characteristics, which determine dynamics of the Sea of Azov. Extreme storm surges in Taganrog Bay and flooding in the Don Delta can be formed under the effect of strong western winds. In this work the sea level oscillations and wind waves in the Taganrog Bay were simulated by means of the coupled SWAN+ADCIRC numerical model, taking into account the flooding and drying mechanisms. The calculations were carried out on an unstructured mesh with high resolution. The wind and atmospheric pressure fields for the extreme storm from 20 to 28 of September, 2014 obtained from WRF regional atmospheric model were used as forcing. The analysis of simulation results showed the following. The western and northern parts of the Don Delta were the most flood-prone during the storm. The size of the flooded area of the Don Delta exceeded 50%. Interaction of storm surge and wind wave accelerated the flooding process, increased the size of the flooded area and led to the intensification of wind waves in the upper of Taganrog Bay due to the general rise of the sea level.

Key words: the Sea of Azov, storm surge, wind waves, flooding, SWAN, ADCIRC, wetting/drying, parallel computing.

I. INTRODUCTION

Storm surges and wind waves are ones of the most important hydrological characteristics, which determine dynamics of the Sea of Azov on synoptic scales. Extreme storm surges of 2–3 m height in Taganrog Bay [1, 2] and flooding in the Don Delta can be formed under the effect of strong western winds. There have been several such cases over the past 20 years: April 12, 1997; March 1, 2005; September 30, 2010; March 24, 2013; September 24, 2014. The two latter cases are described in [2, 3].

In [4], a numerical simulation technology of storm surges and wind waves in the Sea of Azov is presented by means of tightly-coupled SWAN+ADCIRC model [5]. The model validation has shown that it adequately describes the Sea of Azov level variations during intense storms.

Characteristics of storm surge and wind waves in the Taganrog Bay during the extreme storm of September 24–25, 2014, are studied in this work with the mesh of abovementioned technology. High resolution unstructured computational mesh has been created for this purpose. The mesh describes bathymetry and topography of the Don Delta in detail.

II. MODEL DESCRIPTION

The coupled model SWAN+ADCIRC integrates two models – SWAN (Simulation Waves Nearshore) [6, 7] and ADCIRC (Advanced Circulation Model for Shelves Coasts and Estuaries) [8, 9]. Both models are used to simulate the wind waves and storm surge.

The ADCIRC model basic equations are defined as follows

$$\frac{\partial U}{\partial t}+U\frac{\partial U}{\partial x}+V\frac{\partial U}{\partial y}-fV=-g\frac{\partial}{\partial x}\left[\eta+\frac{P_a}{g\rho_0}\right]+\frac{\tau_{sx}-\tau_{bx}}{\rho_0 H}+\frac{M_x-D_x}{H}, \quad (1)$$

$$\frac{\partial V}{\partial t}+U\frac{\partial V}{\partial x}+V\frac{\partial V}{\partial y}+fU=-g\frac{\partial}{\partial y}\left[\eta+\frac{P_a}{g\rho_0}\right]+\frac{\tau_{sy}-\tau_{by}}{\rho_0 H}+\frac{M_y-D_y}{H}, \quad (2)$$

$$\frac{\partial^2\eta}{\partial^2 t}+\tau_0\frac{\partial\eta}{\partial t}+\frac{\partial J_x}{\partial x}+\frac{\partial J_y}{\partial y}-Q_x\frac{\partial\tau_0}{\partial x}-Q_y\frac{\partial\tau_0}{\partial y}=0. \quad (3)$$

Where t is time; x, y are horizontal coordinates; U, V are current velocity components; η is the free surface elevation; f is the Coriolis parameter; g is the gravitation acceleration; P_a is the atmospheric pressure at the surface; ρ_0 is the reference density of water; $H = h + \eta$ is the total water depth; h is the sea bottom; M_x, M_y are the horizontal eddy-viscosity terms; D_x, D_y are terms, obtained after differential transformations of the original system of equations [9]; τ_{bx}, τ_{by} are bottom stress components; τ_0 is the weighting factor that optimizes the phase propagation properties [10]; $Q_x = UH$, $Q_y = VH$ are fluxes per unit width;

$$J_x=-Q_x\frac{\partial U}{\partial x}-Q_y\frac{\partial U}{\partial y}+fQ_y-\frac{g}{2}\frac{\partial\eta^2}{\partial x}-\frac{H}{\rho_0}\frac{\partial P_a}{\partial x}+\frac{\tau_{sx}-\tau_{bx}}{\rho_0}+(M_x-D_x)+\tau_0 Q_x+U\frac{\partial\eta}{\partial t}-gH\frac{\partial\eta}{\partial x};$$

$$J_y=-Q_x\frac{\partial V}{\partial x}-Q_y\frac{\partial V}{\partial y}-fQ_x-\frac{g}{2}\frac{\partial\eta^2}{\partial y}-\frac{H}{\rho_0}\frac{\partial P_a}{\partial y}+\frac{\tau_{sy}-\tau_{by}}{\rho_0}+(M_y-D_y)+\tau_0 Q_y+V\frac{\partial\eta}{\partial t}-gH\frac{\partial\eta}{\partial y}.$$

The following notations are used in (1) – (3):

$$\tau_{sx}=\tau_{sx,wind}+\tau_{sx,wave}, \quad \tau_{sy}=\tau_{sy,wind}+\tau_{sy,wave}, \quad (4)$$

$$\tau_{sx,wind}=\rho_a C_a W_x\sqrt{W_x^2+W_y^2}, \quad \tau_{sy,wind}=\rho_a C_a W_y\sqrt{W_x^2+W_y^2}, \quad (5)$$

$$\tau_{bx}=\rho_0 C_d U\sqrt{U^2+V^2}, \quad \tau_{by}=\rho_0 C_d V\sqrt{U^2+V^2}, \quad (6)$$

where ($\tau_{sx,\,wind}$, $\tau_{sy,\,wind}$) and ($\tau_{sx,\,wave}$, $\tau_{sy,\,wave}$) are surface stresses due to wind and waves, respectively; ρ_a is the air density; W_x, W_y are wind velocity vector components; C_a is the surface stress coefficient; C_d is the bottom stress coefficient.

The stress coefficients in (5) and (6) are given by

$$C_a = 0{,}001\left(0{,}75 + 0{,}067\sqrt{W_x^2 + W_y^2}\right), \qquad C_d = gn^2 / H^{1/3}, \tag{7}$$

where n is Manning's roughness. In general, n is a function of the spatial coordinates and it depends on the type of the underlying surface and the properties of soil and vegetation cover.

SWAN predicts the evolution in geographical space and time of the wave action spectral density $N(x, y, t, \theta, \sigma)$, where θ is the wave direction and σ is the relative frequency, by means of the following equation [6]

$$\frac{\partial N}{\partial t} + \frac{\partial}{\partial x}\left[(c_x + U)N\right] + \frac{\partial}{\partial y}\left[(c_y + V)N\right] + \frac{\partial}{\partial \theta}\left(c_\theta N\right) + \frac{\partial}{\partial \sigma}\left(c_\sigma N\right) = \frac{S_{tot}}{\sigma}, \tag{8}$$

where (c_x, c_y) is the group velocity, c_θ and c_σ are propagation velocities in the θ and σ spaces. The source term S_{tot} denote the wave growth by wind, the action lost due to white-capping, surf breaking and bottom friction, and the action exchanged between spectral components due to the nonlinear effects in deep and shallow water.

SWAN computes wave characteristics by using of fields of wind velocities obtained from atmospheric model, as well as sea level and currents obtained from ADCIRC. In its turn, in ADCIRC wave stresses obtained from SWAN is used, which are given by

$$\tau_{sx,waves} = -\frac{\partial S_{xx}}{\partial x} - \frac{\partial S_{xy}}{\partial y}, \qquad \tau_{sy,waves} = -\frac{\partial S_{xy}}{\partial x} - \frac{\partial S_{yy}}{\partial y}, \tag{9}$$

where S_{xx}, S_{xy}, S_{yy} are wave radiation stresses.

In SWAN model the Grant-Madsen method [11] is used for parameterization of the bottom friction. In this method the bottom roughness scale k_N depends on Manning's roughness n values used in ADCIRC. This is achieved by using relationship $k_N = 30z_0$, where z_0 is defined as [12]

$$z_0 = H \exp\left[-\left(1 + 0{,}4\frac{H^{1/6}}{n\sqrt{g}}\right)\right]. \tag{10}$$

SWAN and ADCIRC are executed sequentially on the same unstructured grid and use the same set of computational cores. Both models use Message Passing Interface (MPI), which allows the use of parallel computing.

The coupled model allows to introduce the total sea level (TSL) as a sum:

$$\mathrm{TSL} = \mathrm{SL} + \mathrm{CW}, \tag{11}$$

where $\mathrm{SL} = \eta$ is the sea level variations due to the combined effect of wind stresses, atmospheric pressure and wave stresses; $\mathrm{CW} = H_s/2$ is the height of wind wave crests; H_s is the significant wave

height (SWH) from SWAN. Actually, the TSL gives more adequate estimation of the sea level variations, since it includes both low- and high-frequency components.

III. RESULTS OF NUMERICAL EXPERIMENTS AND DISCUSSION

In numerical experiments a finite element mesh comprised of 178 565 nodes (348 735 triangular elements) was utilized. The mesh included the Sea of Azov and Kerch Strait (Fig. 1). The size of triangular elements edges varies from 50 to 800 m. Integration time steps in ADCIRC and SWAN were 1 s and 600 s respectively. The angular resolution in SWAN was set to 10°. A grid with 40 nodes was used for frequency coordinate in the range of 0.03 – 1.4 Hz. Two values were used for Manning's roughness: 0.025 for the sea bottom; 0.10 for the land. The weighting coefficient τ_0 is defined by: $\tau_0 = 0.03 + 1.5 C_d \sqrt{U^2 + V^2} / H$.

ADCIRC has 2 tuning parameters: $H_{\min}$ is the minimal water depth at which the calculated cell is inactive and removed from the calculations; $U_{\min}$ is the minimal velocity at which the cell is opened for flooding. According to [13], these parameters are set to be 0.1 m and 0.01 m/s respectively. The impact of the river discharge on the Don Delta flooding was not considered. A radiation condition was used on the southern border of the Kerch Strait.

A series of numerical experiments on modeling of wind waves and the Sea of Azov level was carried out for the extreme storm situation, which happened on September 24–25, 2014, and was caused by the passage over the sea of fast and deep cyclone, which was formed in the western part of the Black Sea.

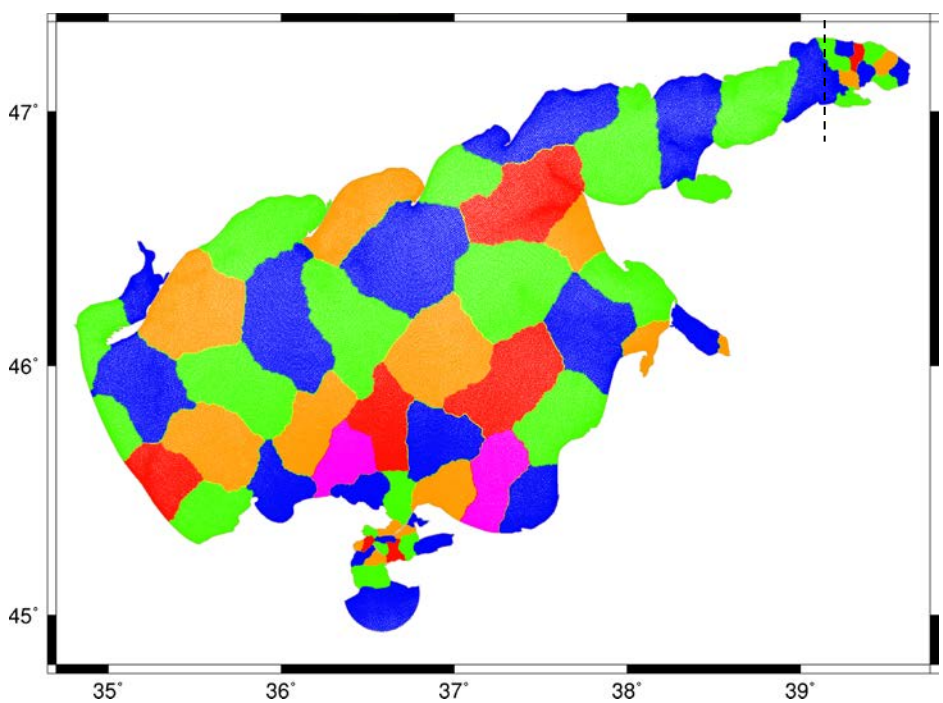

Fig. 1. Finite element mesh for the Sea of Azov. Colors indicate local sub-meshes and shared boundary layers (domain decomposition for 64 computational cores).

Surface wind and atmospheric pressure fields with spatial resolution of 7 km and time resolution of 3 hours from the WRF regional model (ecobase.org.ua) for the period from 20 to 28 of September 2014 were used as atmospheric forcing. According to the WRF data, the maximum wind speed in the Taganrog Bay during the specified time period varied from 17 m/s in the Don Delta area up to 21 m/s in Dolzhansky Strait.

Figure 2 shows the time variations of wind speed and wind direction from the WRF model for the Don delta for the period from 20 to 28 of September 2014. The wind direction is measured counter-clockwise in relation to the *x*-axis, which points to the east. As it can be seen, during the first 90 hours the wind was predominantly eastern and south-eastern with the velocity of 7.5 m/s. Next day the wind velocity increased to 17 m/s. Then there was a sharp change of wind direction from south-eastern to western, which created suitable conditions for the formation of strong storm surge at th**e** upper of Taganrog Bay.

Numerical experiments were carried out with zero initial conditions. In the first experiment (E1), the coupling between ADCIRC and SWAN was off, and thus, mechanisms of interaction between currents, sea level and wind waves were not taken into account. These mechanisms were accounted for in the second experiment (E2). In the experiment E1 bottom roughness scale $k_N = 0.01$ m was used. In the experiment E2 $k_N = 30z_0$, where z_0 is defined by the relationship (10).

The analysis of the results of numerical experiments shows that overall sea level decrease and damped oscillations on its background took place in the bay during the first 3,5 days. Sea level rise began in the first half of September, 24, due to a sharp change in wind direction from offshore to onshore. Starting from September, 25, the wind velocity began to decrease, leading to a gradual sea level fall in the bay.

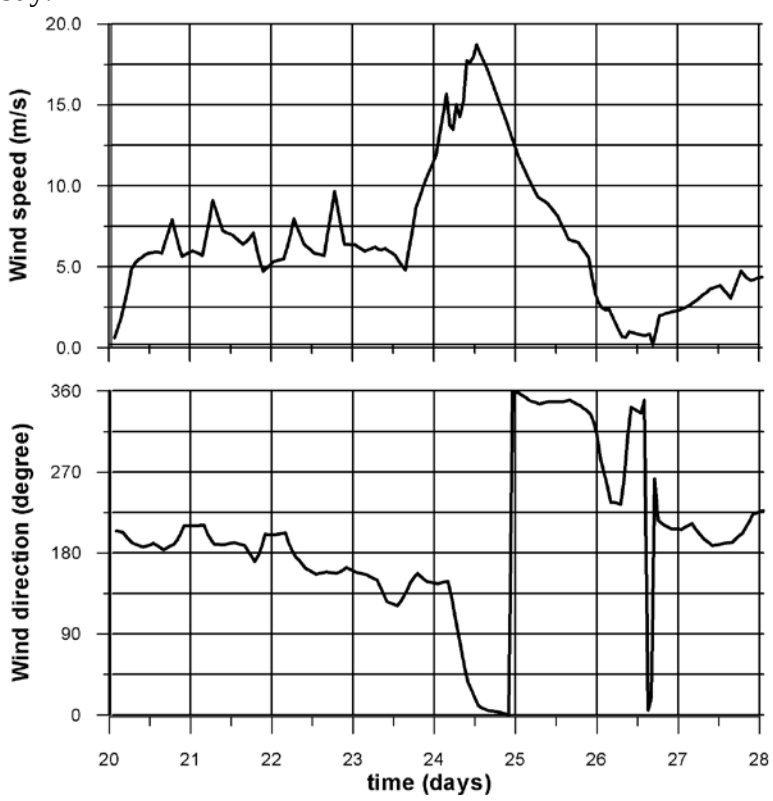

Fig. 2. Time series of the simulated wind velocity and wind direction in the Don delta for the period 20–28 of September 2014.

Fig. 3 shows the Don Delta flooding extent for four characteristic moments of time. The following procedure was developed for construction of these fields. The dynamic depth H in all cell points was compared with constant $H_{\min}$ at any time. If all three cell nodes satisfied the condition $H > H_{\min}$ at the same time, than the cell was considered to be flooded. As can be seen, notable flooding regions in the Don delta began to appear, starting from September, 25. Western and northern parts of the delta turned out to be more vulnerable to flooding.

The flooding index (FI) was used to evaluate changes of the flooded area size in the Don Delta over time:

$$\mathrm{FI}(t) = \left(1 - \frac{S(t)}{S(0)}\right) \cdot 100\%, \quad S(t) = \iint_{\Omega} \delta_d(x, y, t)\,dxdy, \quad \delta_d(x, y, t) = \begin{cases} 1, & H(x, y, t) \le H_{\min} \\ 0, & H(x, y, t) > H_{\min} \end{cases}, \quad (12)$$

where $S(t)$ is the size of dry land at a moment t in time; $S(0)$ is the area of dry land at initial time. $H_{\min}$ is the minimum depth in the wetting and drying algorithm. In (12), the integration is performed in the Ω region, the western boundary of which is represented by a vertical dashed line on Fig. 1. The flooding index represents variation of the sum of all dry areas in the Don delta over time in percentage. If bottom dries, then $S(t) > S(0)$ and the flooding index becomes negative.

Fig. 4 shows the dependence of the flooding index on time for the period from 20 to 28 September, 2015. The blue curve represents the E1 experiment, the red curve represents the E2 experiment. As it can be seen, the sea level decreased from 20 to 23 September. This manifested itself in a periodic increase of the dry land area by 5–8%. Then, after the change of wind direction, a sharp flooding of the delta began, and in the next 24 hours the delta area decreased by about 40%. Following that, the flooding rate decreased and the dry land area dropped by 10% within next two days. Comparison of the curves in Fig. 4 shows that the coupling accelerates the process of flooding and increases flooding of the delta area by 4%.

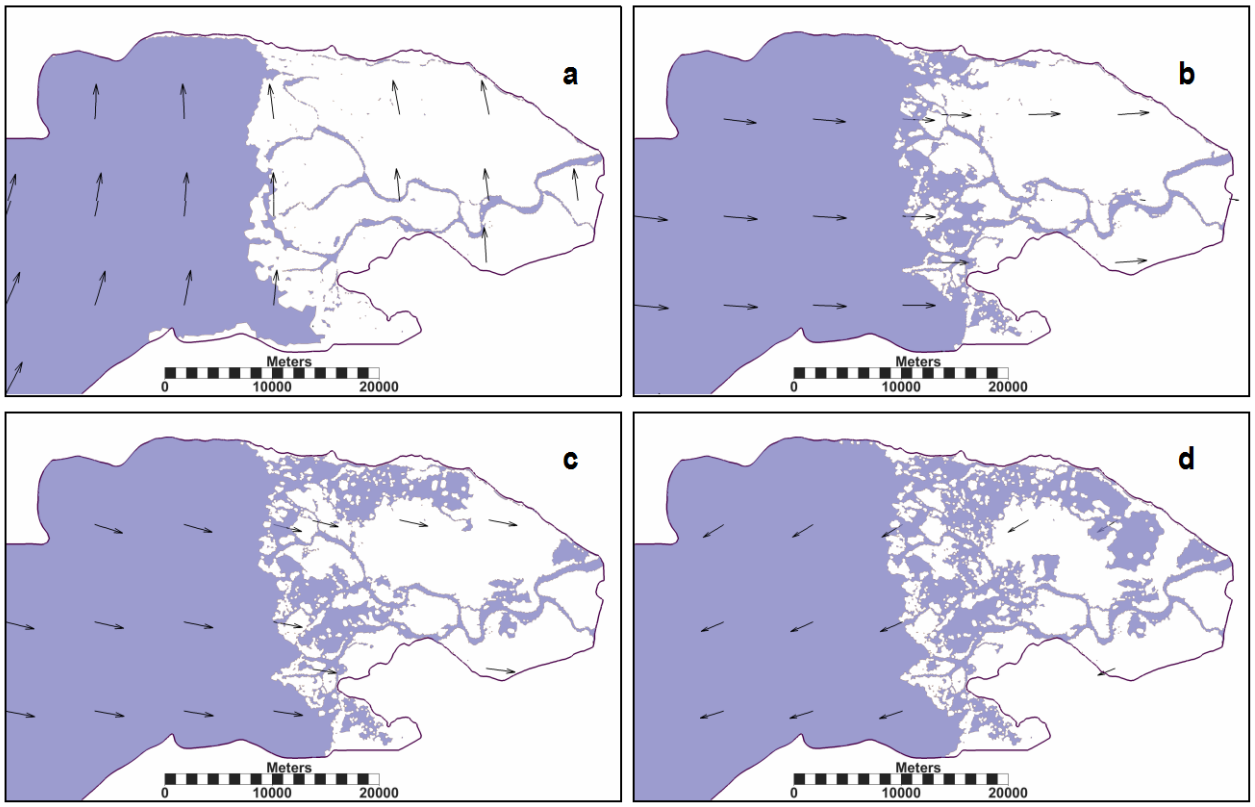

Fig. 3. Flooding extent of the Don Delta and wind directions: (a) September,24, 2014 at 00:00; (b) September, 25, 2014 at 00:00; (c) September 25, 2014 at 12:00; (d) September 27, 2014 at 00:00.

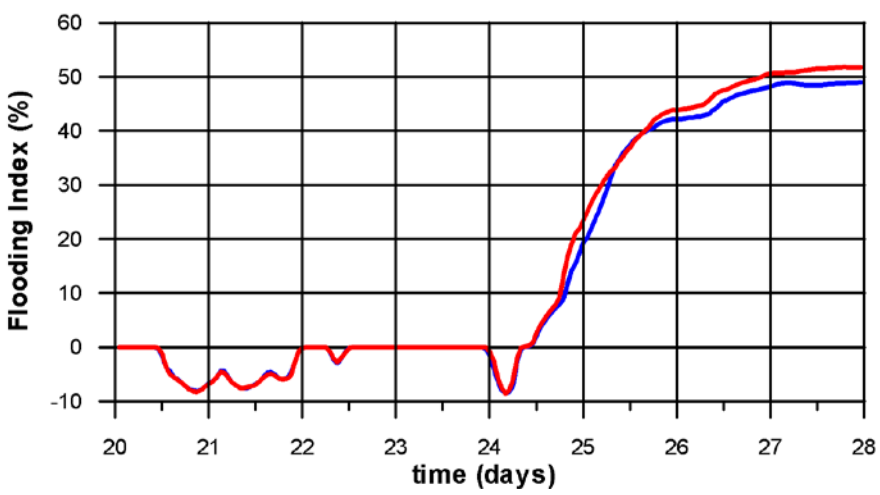

Fig. 4. FI *time series for the period 20–28 of September 2014 (blue line – E1 experiment, red line – E2 experiment).*

The following formulas are used for the estimation of mean values SL, SWH and TSL:

$$\mathrm{SL_m}(t) = \frac{\iint\limits_{\Omega} \mathrm{SL}(x,y,t)\cdot\delta_w(x,y,t)dxdy}{\iint\limits_{\Omega} \delta_w(x,y,t)dxdy}, \tag{13}$$

$$\mathrm{SWH_m}(t) = \frac{\iint\limits_{\Omega} \mathrm{SWH}(x,y,t)\cdot\delta_w(x,y,t)dxdy}{\iint\limits_{\Omega} \delta_w(x,y,t)dxdy}, \tag{14}$$

$$\mathrm{TSL_m}(t) = \frac{\iint\limits_{\Omega} \mathrm{TSL}(x,y,t)\cdot\delta_w(x,y,t)dxdy}{\iint\limits_{\Omega} \delta_w(x,y,t)dxdy}, \tag{15}$$

where $\delta_w(x,y,t) = \begin{cases} 0, & H(x,y,t) \le H_{\min} \\ 1, & H(x,y,t) > H_{\min} \end{cases}$.

Fig. 5 shows SL_m functions of time for the E1 experiment (blue curve) and the E2 experiment (red curve). In the E2 experiment, SL_m values at all points are 5–6 cm higher than the corresponding SL_m maximum values in the E1 experiment. Thus, the contribution of wave stress to the sea level elevation is insignificant for the given water area.

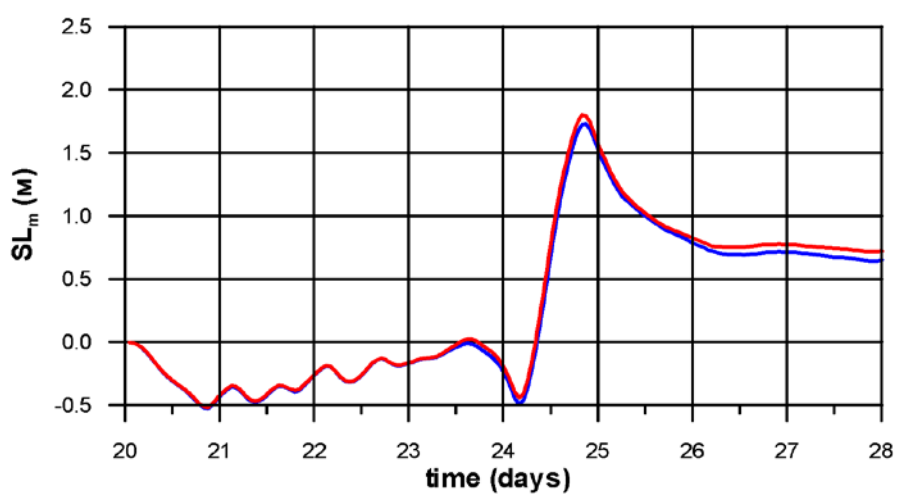

Fig. 5. $\mathrm{SL_m}$ *time series for the period 20–28 of September 2014 (blue line – E1 experiment, red line – E2 experiment).*

Fig. 6 shows $\mathrm{SWH_m}$ functions of time for the E1 (blue curve) and E2 (red curve) experiments. As it can be seen, the E2 experiment gives more intense wind waves in comparison with the E1 experiment for the stormy period (24–25 of September). $\mathrm{SWH_m}$ maximum is 35% higher for the E2 experiment than for the E1 experiment. To determine the causes of this effect, an additional numerical experiment (E3) was carried out, in which SL was not taken into account in

SWAN in contrast to the E2. The dependence of $\mathrm{SWH_m}$ on time for the E3 experiment is shown by the black dashed curve. It is almost the same as the curve for the E1 experiment.

The physical meaning of this result is obvious. There are areas with shallow depths at the top of the Taganrog Bay, where wind waves cannot be significant due to strong dissipative effects. At the same time, as the sea level rises by 1.5–2 m and more the dynamic depth can significantly increase in these areas. This will facilitate increase of wave heights as a result of bottom friction influence reduction.

Thus, the storm surge creates conditions for the intensification of wind waves in the bay due to the general rise of the sea level. It is natural to assume that it is the combination of strong wind surges and intense wind waves that creates one of the main mechanisms of the extreme level rises in the Taganrog Bay, which leads to the flooding of the Don Delta.

Time dependence of TSL_m for the E2 experiment is shown in Fig. 7. As it can be seen, the maximum value of $\mathrm{TSL}_m = 2.25$ m is reached on September, 24, in the afternoon. This fits well with the measurements at hydro-meteorological station Taganrog, where the maximum level of 2.5 m was observed on September, 24, at 18.00. Comparison of the curves in Fig. 7 and Fig. 5 shows that contribution of wind waves to the full level reaches 20% during the maximum of the storm.

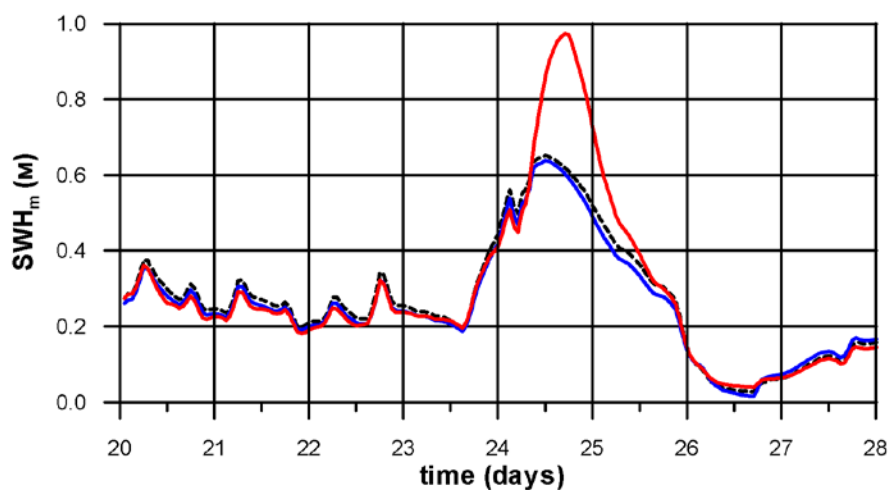

Fig. 6. SWH_m *time series for the period 20–28 of September 2014 (blue line – E1 experiment, red line – E2 experiment, black dashed line– E3 experiment).*

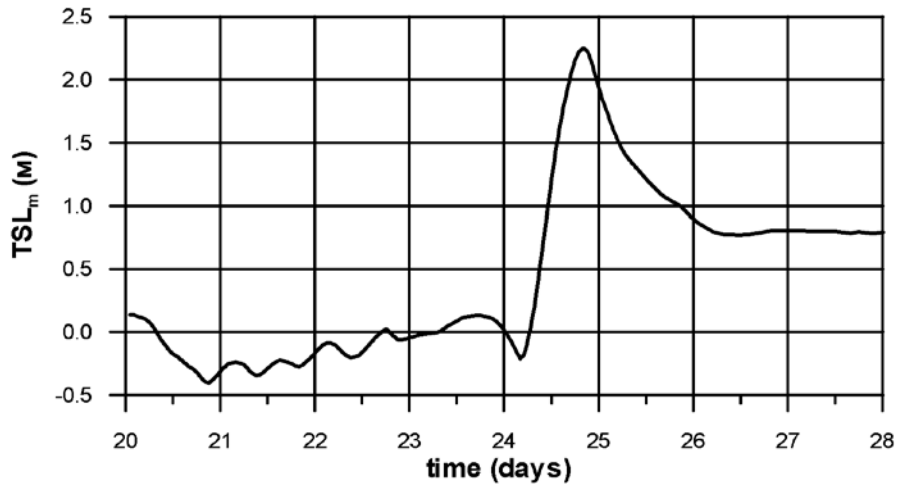

Fig. 7. TSL$_m$ *time series for the period 20–28 of September 2014 (E2 experiment).*

IV. Conclusion

The sea level oscillations and wind waves in the Taganrog Bay were simulated by means of the coupled SWAN+ADCIRC numerical model, taking into account the flooding and drying mechanisms. The calculations were carried out on an unstructured mesh with high resolution. The wind and atmospheric pressure fields for the extreme storm from 20 to 28 of September, 2014 obtained from WRF regional atmospheric model were used as forcing.

The analysis of simulation results showed the following. The western and northern parts of the Don Delta were the most flood-prone during the storm. The size of the flooded area of the Don Delta exceeded 50%. Interaction of storm surge and wind wave accelerated the flooding process, increased the size of the flooded area and led to the intensification of wind waves in the upper of Taganrog bay due to the general rise of the sea level. Wave stress did not contribute significantly to the value of storm surge.

V. Acknowledgment

This work was supported by RFBR, research project No. 15-05-06382 A.

The authors thank Crystal Fulcher from UNC-Institute of Marine Sciences for providing the source codes of SWAN+ADCIRC.

Calculations were carried out on a computing cluster of Marine Hydrophysical Institute and "Lomonosov" supercomputer of Moscow State University. Some ADCIRC visualizations were produced with FigureGen (Dietrich et al., 2013).

VI. References

[1] V.A. Ivanov, V.V. Fomin, "*Mathematical Modelling of Dynamical Processes in the Sea-Land Area*", Kyiv: Akademperiodyka, 2010, 286 p.

[2] G.G. Matishov "The Kerch Strait and the Don Delta: the Security of Communications and Population", *Vestnik Yuzhnogo Nauchnogo Tsentra*, 11(1), 2015, pp. 6 – 15. (In Russian).

[3] G.G. Matishov, A.L. Chikin, S.V. Berdnikov, I.V. Sheverdyaev, A.V. Kleshchenkov et al., "Extreme flooding of the Don Delta in spring 2013: chronology, formation conditions, and consequences", *Vestnik Yuzhnogo Nauchnogo Tsentra*, 10(1), 2014. pp. 17–24. (In Russian).

[4] V.V. Fomin, A.A. Polozok, R.V Kamyshnikov, “Wave and Storm Surge Modelling for Sea of Azov with use of ADCIRC+SWAN”, *Collection of articles of the II International conference «Geoinformation Sciences and Environmental Development: New Approaches, Methods, Technologies»*, Rostov-on-Don, 2014, pp. 111 – 116.

[5] J.C. Dietrich, M. Zijlema, J.J. Westerink, L.H. Holthuijsen , C. Dawson, et al., “Modeling Hurricane Waves and Storm Surge using Integrally-Coupled, Scalable Computations”, *Coastal Engineering*, vol. 58, No. 1, 2011, pp. 45 – 65.

[6] N. Booij, R.C. Ris, L.H. Holthuijsen “A third-generation wave model for coastal regions. Model description and validation”, *J. Geophys. Res*., 104 (C4), 1999, pp. 7649 – 7666.

[7] M. Zijlema, “Computation of wind-wave spectra in coastal waters with SWAN on unstructured grids”, *Coastal Engineering*, vol. 57, No. 3, 2010, pp. 267 – 277.

[8] R.A. Luettich, J.J. Westerink, “*Formulation and Numerical Implementation of the 2D/3D ADCIRC*”, 2004, URL: http://adcirc.org/adcirc_theory_2004_12_08.pdf.

[9] R.A. Luettich, J.J. Westerink, N.W. Scheffner, *“ADCIRC: an advanced three-dimensional circulation model for shelves coasts and estuaries, report 1: theory and methodology of ADCIRC-2DDI and ADCIRC-3DL”*, Dredging Research Program Technical Report DRP-92-6, U.S. Army Engineers Waterways Experiment Station, Vicksburg, MS, 1992, 137 p.

[10] J.H. Atkinson, J.J. Westerink, J.M. Hervouet, “Similarities between the wave equation and the quasi-bubble solutions to the shallow water equations”, *International Journal for Numerical Methods in Fluids*, vol. 45, 2004, 689–714.

[11] W.D. Grant, O.S. Madsen, “Movable bed roughness in unsteady oscillatory flow”, *J. Geophys. Res.*, vol. 87, 1982, pp. 469 – 481.

[12] P.C. Kerr, R.C. Martyr, A.S. Donahue, M.E. Hope, J.J. Westerink, et al., “U.S. IOOS coastal and ocean modeling testbed: Evaluation of tide, wave and hurricane surge response sensitivities to mesh resolution and friction in the Gulf of Mexico”, *J. Geophys. Res. Oceans*, 118, 2013, pp. 4633 – 4661, doi:10.1002/jgrc.20305.

[13] J.C. Dietrich, R.L. Kolar, R.A. Luettich, “Assessment of ADCIRC's Wetting and Drying Algorithm”, Proceedings of the XV International Conference on Computational Methods in Water Resources, vol. 2, 2004, pp. 1767 – 177.